Journal of Basics and Applied Sciences Research (JOBASR)
ISSN (print): 3026-9091, ISSN (online): 1597-9962
Volume 4(4) July 2026
DOI: https://dx.doi.org/10.4314/jobasr.v4i4.6

Metal-Coordinated Aldazine Schiff Base: Synthesis, Spectroscopic Characterisation, and Evaluation of Antimicrobial and Antioxidant Potentials of CU (II), ZN (II) and AG(I) Complexes

Oluseyije, O. J.[1*] & Olalekan, T. E.[2]
[1,2]Department of Chemistry, University of Ibadan, Ibadan 200285, Oyo State, Nigeria
[*]Corresponding Author Email: topeolalekan11@yahoo.com

ABSTRACT
Antimicrobial resistance poses a growing threat to global health as multidrug-resistant pathogens render many conventional drugs ineffective. This has created an urgent need for alternative therapeutic approaches. In response, an aldazine Schiff base and Cu(II), Zn(II) and Ag(I) complexes were synthesised, spectroscopically characterised and evaluated for antimicrobial and antioxidant potentials. The ligand, **3EHH**, was prepared from hydrazine and 3-ethoxy-2-hydroxybenzaldehyde. The Cu(II) (**Cu3E**), Zn(II) (**Zn3E**), and Ag(I) (**$Ag_2$3E**) complexes were synthesised and characterised by magnetic moments, NMR, IR and UV/Vis spectra. The *in vitro* antimicrobial and antioxidant properties were investigated using agar well diffusion, DPPH radical scavenging and ferric reducing antioxidant power (FRAP) assays, respectively. Formation of **3EHH** was confirmed by the *bis*-azomethine protons signal at 8.69 δ ppm and the absence of amino and carbonyl protons. Coordination via azine nitrogen and phenolate oxygen was supported by shifts in *ν*(C=N) from 1622 to 1631–1616 cm^{-1} and *ν*(C–O) from 1214 to 1210–1193 cm^{-1}, loss of phenolic protons in **Zn3E** NMR spectrum, and changes in π→π* transitions, together with new LMCT (423–405 nm) and d→d bands (662 nm) in the UV-Visible spectra. The inhibition zones and MIC were in the ranges of 8–24 mm and 10–0.125 mg/mL, respectively. The DPPH and FRAP antioxidant assays showed IC_{50} 138.62–486.82 µg/mL and 9.240–22.890 AAE mg/g at 1000 µg/mL, respectively. Chelation of **3EHH** with Cu (II), Zn(II), and Ag(I) improved its bioactivity, with the Cu (II) complex showing the greatest potential as a dual antimicrobial and antioxidant agent.

Keywords:
Tetradentate ligand;
LMCT band;
Antimicrobial and
Antioxidant activity

INTRODUCTION

Schiff bases represent one of the most significant classes of ligands in coordination chemistry due to their facile synthesis, structural versatility and diverse applications (Dhanya, *et al*., 2025; Rani *et al*., 2026; Saulawa *et al*., 2024; Thakor *et al*., 2024). *Bis*-Schiff bases are organic compounds containing two imine −CH=N− groups linked by a spacer unit. They are typically synthesized through the condensation of a diamine with two equivalents of an aldehyde or ketone. These compounds have attracted significant interest across catalysis, material science, and medicinal chemistry due to their straightforward preparation, structural diversity, coordination ability and enhanced biological activities (Chouiter *et al*., 2023; Rabiei *et al*., 2023, Rajadurai *et al*., 2026, Hadigheh Rezvan & Aminivand, 2024; Hasan *et al*., 2023; Taha *et al*., 2023).

Azines are a specific subclass of *bis*-Schiff bases characterised by a central −C=N−N=C− linkage formed from the condensation of hydrazine with two carbonyl compounds. They are referred to as aldazines and ketazines when derived from aldehydes and ketones, respectively.

Salicylaldehyde-based azines are particularly well studied because the *ortho*-hydroxyl group provides an N_2O_2 donor set, promotes intramolecular hydrogen bonding, and enhances stability and metal chelation. In combination with their metal complexes, they have been explored for biological potency and their notable photophysical properties (Chosenyah *et al*., 2026; Ganesan *et al*., 2024; Gorokhov *et al*., 2024; Karimian *et al*., 2021; Liu *et al*., 2022; Naito *et al*., 2025; Sahu *et al*., 2022).

How to cite this article: Oluseyije, O. J. & Olalekan, T. E. (2026). Metal-Coordinated Aldazine Schiff Base: Synthesis, Spectroscopic Characterisation, and Evaluation of Antimicrobial and Antioxidant Potentials of CU (II), ZN (II) and AG(I) Complexes. *Journal of Basics and Applied Sciences Research*, *4*(4), 48-58. https://dx.doi.org/10.4314/jobasr.v4i4.6

Despite the extensive work on salicylaldehyde-based azines, those derived specifically from 3-ethoxysalicylaldehyde remain largely underexplored. The introduction of an ethoxy group at the 3-position offers potential to modulate solubility, electronic properties, and coordination behaviour (Aazam *et al*., 2024; Shaaban *et al*., 2025). The synthesis and characterisation of 3-ethoxysalicylaldimine azine and its supramolecular Zn(II) and Co(III) complexes were reported by Liu *et al* (2015) and Mathivanan *et al* (2024). In this context, this study focused on the synthesis and spectral characterisation of Cu(II), Zn(II), and Ag(I) complexes of the 3-ethoxy-2-hydroxybenzaldehyde azine. The antimicrobial potency of the ligand and the metal complexes was investigated against the chosen bacterial and fungal strains, and their antioxidant property was investigated using the DPPH radical scavenging and FRAP methods.

MATERIALS AND METHODS

Materials

All chemicals were purchased from commercial suppliers and were used as received. Uncorrected melting points were determined on a Gallen Kamp melting point apparatus. Infrared spectra were recorded as nujol mulls on a PerkinElmer FT-IR spectrophotometer in the range between 4000 and 400 cm^{-1}. The UV-Vis electronic spectra were obtained on a PerkinElmer Lambda 25 UV/Vis spectrometer in DMF solutions at 10^{-3}–10^{-5} M concentrations in the range 190–900 nm. ^{1}H and ^{13}C NMR spectra were obtained in $(CD_3)_2SO$ on Bruker Avance 400 MHz NMR spectrometer, with reference to TMS. Percentage metal analysis of the acid-digested samples was determined using EDTA titrimetry method.

Synthesis of 3EHH

The ligand was synthesised as shown in Scheme 1, by heating a solution containing hydrazine monohydrate (0.3906 mg, 7.802 mmol), 3-ethoxy-2-hydroxybenzaldehyde (1.2965 g, 7.802 mmol) and four drops of acetic acid to reflux in 15 mL EtOH in a round-bottom flask for 2 h. The reaction was monitored by TLC. Upon completion and cooling, the mixture was filtered to obtain a yellow precipitate, which was washed with ethanol, then diethyl ether, and allowed to dry in air. Yield: 0.9096 g (71%), Mp 195-197°C, mol. wt: 328.37. ^{1}H-NMR (400 MHz, $CDCl_3$): δ = 11.56 (s, 2H, -OH), 8.66 (s, 2H, -CH=N-), 6.99 (t, 4H, 4a,b, 6a,b, *J* = 8.0 Hz), 6.89 (t, 2H, 5a,b, *J* = 8.0 Hz), 4.15 (q, 2H, -C**H**$_2$-CH_3, *J* = 8.0 Hz), 1.52 (t, 3H, -CH_2-C**H**$_3$, *J* = 4.0 Hz). ^{13}C NMR (400 MHz, $CDCl_3$): δ = 164.72 (C=N), 150.01 ($C_{2a,b}$), 147.62 ($C_{3a,b}$), 124.11 ($C_{6a,b}$), 119.39 ($C_{1a,b}$), 117.49 ($C_{4a,b}$), 116.70 ($C_{5a,b}$), 64.74 (-**C**H_2-CH_3), 14.89 (-CH_2-**C**H_3) ppm.

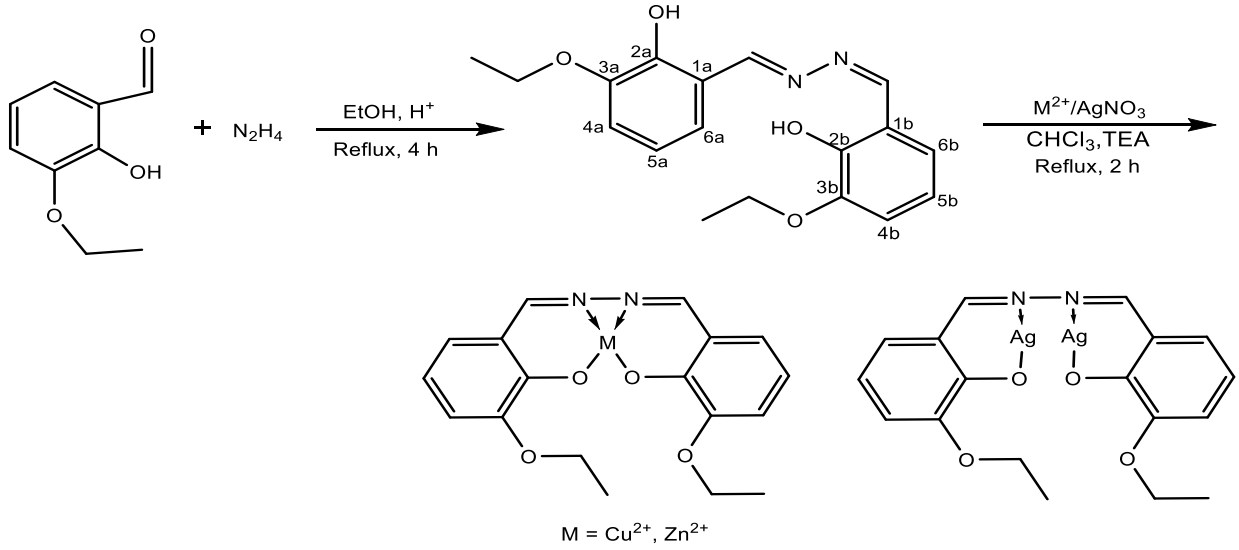

Scheme 1: Synthesis of the 3EHH Schiff base and metal complexes

Synthesis of metal complexes

The general method for the preparation of the metal complexes is shown in Scheme 1. The ligand, **3EHH** (0.20 mg, 1.1098 mmol) was dissolved in 10 mL chloroform in a round-bottom flask, to which three drops of triethylamine were added, and stirred for 10 min. $Zn(OAc)_2.2H_2O$ (0.1218 g, 0.5549 mmol), in 10 mL hot ethanol was added in drops to the ligand solution, after which the mixture turned dark brown and was refluxed for 2 h. After cooling to ambient temperature, the mixture was filtered to obtain the precipitate, which was washed with ethanol and diethyl ether, and allowed to dry in air. The brown product was weighed as 0.2009 g. ^{1}H-NMR (400 MHz, DMSO-d_6): δ = 8.43 (s, 2H, -CH=N-), 6.79 (d, 4H, 4a,b, 6a,b, *J* = 4.0 Hz), 6.33 (t, 2H, 5a,b, *J* = 8.0 Hz), 4.01 (q, 2H, -C**H**$_2$-CH_3, *J* = 4.0 Hz, *J* = 8.0 Hz), 1.33 (t,

3H, -CH_2-C**H**$_3$, J = 8.0 Hz). ^{13}C NMR (400 MHz, DMSO-d_6): δ = 168.55 (-CH=N-), 163.02 ($C_{3a,b}$), 151.81 ($C_{2a,b}$), 127.18 ($C_{5a,b}$), 119.39 ($C_{6a,b}$), 116.22 ($C_{4a,b}$), 111.49 ($C_{1a,b}$), 63.98 (-**C**H_2-CH_3), 15.53 (-CH_2-**C**H_3) ppm.

The Cu(II) and Ag(I) complexes were similarly prepared using the same amount of **3EHH**, with $CuCl_2 \cdot 2H_2O$ (0.1892 g, 1.1098 mmol) and $AgNO_3$ (0.1885 g, 1.1098 mmol) to derive the masses of 0.1680 g and 0.2420 g, respectively. The yields and other analytical data of the compounds were recorded in **Table 1**.

In vitro antibacterial assay procedure

The *in vitro* antibacterial activity of the synthesised compounds was evaluated using the agar well diffusion method. The screening was performed using six bacterial strains and two fungal strains, including the Gram-positive *Staphylococcus aureus* ATCC 6571 and *Bacillus subtilis* ATCC 3366, Gram-negative *Escherichia coli* ATCC 25922, *Klebsiella pneumoniea* ATCC 700303, *Salmonella typhi* ATCC 14028 and *Pseudomonas aeruginosa* ATCC 27853; *Candida albicans* and *Trichophyton rubrum*. Ciprofloxacin (10 µg/mL) and ketoconazole (1 mg/mL, 1%) served as the reference antibacterial and antifungal drugs, respectively, while DMF was employed as the diluent and the negative control.

Preparation of microbial inocula and nutrient agar followed standard protocols. Sterilised Mueller Hinton Agar (20 mL) was aseptically dispensed into sterile petri dishes. The agar was allowed to set for 10 minutes, after which the petri dishes containing the agar were dried in a hot air oven to remove moisture from the cover of the plate and from the surface of the agar. Using the spread plate method, 10^{-5} dilution of an 18-hour broth adjusted to 0.5 McFarlan standard was spread on the surface of the agar using a sterile cotton swab. A flamed 6mm-diameter cork-borer was allowed to cool, after which sized-wells were made in the inoculated agar. The already prepared different concentrations of the samples were added (100 µL) to each hole and labelled appropriately. Similar volumes of the controls were added separately to the wells, and the plates were left for an hour to allow for proper diffusion of the samples and then incubated at 37°C for 24 h (for bacteria) or at 25°C for 72 h (for fungi) (NCCLS, 1999; 2002). After cooling, the diameters of inhibition zones were measured in mm.

Determination of Minimum Inhibitory Concentration (MIC)

The MIC was determined using broth micro dilution method. The synthesised samples were dissolved in double strength Tryptone soya broth to obtain solutions of 4 mg/mL and 2 mg/mL concentrations, from which 100 µL was added into each well. Ciprofloxacin (10 µg/mL) was also diluted to obtain a lower 5 µg/mL concentration, while additional lower concentrations of ketoconazole (1 to 0.25 mg/mL) were prepared, and these were separately added to the wells. Each well content was inoculated with 10 µL of microorganism solution and the microplates were incubated. The least concentration which showed no turbidity or growth was taken as the MIC.

Determination of Minimum Microbiocidal Concentration (MMC)

After checking for growth or turbidity in the test plates (MIC determination), 10 µL of 0.2 mg/mL of *p*-INT solution (*p*-iodonitrotetrazolium violet) was added to the wells that showed no growth or turbidity. The plates were then further incubated at 37°C for 30 min. Wells with colour change from yellow to pinkish red were an indication of microbial growth. The least concentration which showed no trace of growth was taken as the minimum bactericidal concentration (MBC) or the minimum fungicidal concentration (MFC).

Antioxidant Assay Procedure

DPPH radical scavenging activity assay

The molecule, 2,2-diphenyl-1-picrylhydrazyl (DPPH) is characterised as a stable free radical by its delocalised electron, which also gives rise to the deep violet colour, resulting from an absorption band in methanol solution, centred at about 517 nm (Blois, 1958). When a solution of DPPH is mixed with that of a substrate (AH) that can donate a hydrogen atom, this would give rise to its reduced form with the loss of this violet colour. In order to evaluate the antioxidant potential through free radical scavenging by the test samples, the change in optical density of DPPH is monitored (Brand-Williams *et al.*, 1995). The samples and ascorbic acid standard were each dissolved in DMF to derive 1 mg/mL concentration, and diluted with 1 mL of 0.3 mM DPPH solution and after 30 min, the absorbance of each mixture was measured at 517 nm (Manzocco *et al*., 1998). The percentage of the DPPH radical scavenging was calculated using the equation:

$$\%\ \text{inhibition} = \frac{\text{Control(A)} - \text{Sample(A)}}{\text{Control(A)}}\ X\ 100\%$$

where Control(A) is the absorbance of control DPPH, and Sample(A) is the absorbance of the sample where the reaction has taken place.

Ferric Reducing Antioxidant Power (FRAP) Assay

Ferric reducing antioxidant power was measured according to the method of Oyaizu (1986) with a slight modification. Each compound was mixed with 2.5 mL of 20 mM phosphate buffer and 2.5 mL 1% w/v potassium ferricyanide, and the mixture was incubated at 50°C for 30 min. Afterwards, 2.5 mL of 10% w/v trichloroacetic acid and 0.5 mL 0.1% w/v ferric chloride were added to the mixture, and left to stand for 10 min. Ascorbic acid was used as the positive control and the absorbance values were measured at 700 nm. The assays were run in triplicate.

RESULTS AND DISCUSSION

Analytical analyses

The analytical data of **3EHH** and the complexes were shown in **Table 1**. The complexes **Cu3E**, **Zn3E** and **Ag$_2$3E** precipitated as brown, yellow and green powders, respectively. They were stable in air and obtained in 35-93% yields. The ligand and the metal complexes were soluble in DMF and DMSO. The compounds were also thermal stable and melted at 196°C (**3EHH**), 178°C (**ZnE**) and >220°C (**Ag$_2$3E**). The stoichiometry of the Cu(II) and Zn(II) complexes was determined by the percentage metal content of the Cu(II) and Zn(II) complexes, which gave close experimental and calculated values.

Table 1: Analytical table for the compounds

Compounds	Mol. Wt (g mol^{-1})	Colour	M.Pt (°C)	Yield %	% Metal Exp (Cal)
3EHH	328.37	Yellow	195-197	71	----
[**Cu3E**].6H$_2$O	481.32	Brown	222-224	35	12.71 (12.86)
[**Zn3E**].5H$_2$O	481.08	Yellow	177-180	92	13.13 (13.57)
[**Ag$_2$3E**]	485.94	Pale green	255-258^D	93	----

D, decomposition temperature

^{1}H and ^{13}C NMR spectra

The ^{1}H and ^{13}C NMR spectra of **3EHH** and **Zn3E** were obtained in $CDCl_3$ and DMSO-d_6, respectively, and were presented in **Figures 1-4**. The phenolic and azomethine protons of **3EHH** were seen as singlet peaks at δ 11.56 ppm and δ 8.67 ppm, respectively. The aromatic protons resonated at δ 6.99 (*t*) and 6.89 (*t*), in consistence with their positions on the substituted aromatic rings. The quartet and triplet peaks at δ 4.15 ppm and δ 1.52 ppm were assigned to the ethoxy -CH_2 and -CH_3 protons, respectively. The azomethine, methine and methyl carbon atoms resonated at δ 164.72 ppm, 64.74 and δ 14.89 ppm, respectively, and the absorptions for the aromatic carbon atoms occurred in the range δ 116.70–150.01 ppm as expected. These values were in consistence with those reported by similar compounds (Liu *et al*., 2024; Mathivanan *et al*., 2024).

In the ^{1}H NMR spectrum of **Zn3E**, the disappearance of the singlet peaks at 11.56 δ ppm indicated deprotonation, thereby confirming coordination to Zn^{2+} through the phenolate oxygen. The distinct singlet and multiple peaks at 8.43 ppm and δ 6.79 and 6.33 ppm were assigned to the azomethine and aromatic protons, while the quartet/triplet peaks of ethoxy protons appeared in the upfield region at δ 4.01 and 1.33 ppm. The ^{13}C NMR spectrum of **Zn3E** showed the azomethine and aromatic carbon atoms resonances in the upfield region between 168.55 and 111.49 δ ppm, while the sp^3 carbon atoms absorbed at 63.98 and 56.44 δ ppm. The upfield shifts in resonances of carbon atoms bonded to the donor atoms were observed for -CH=N- (164.72 to 168.55 δ ppm) and C_2 (150.01 to 163.02 δ ppm). This resulted from the shielding effect of the Zn^{2+} ion in the ligand system upon complexation.

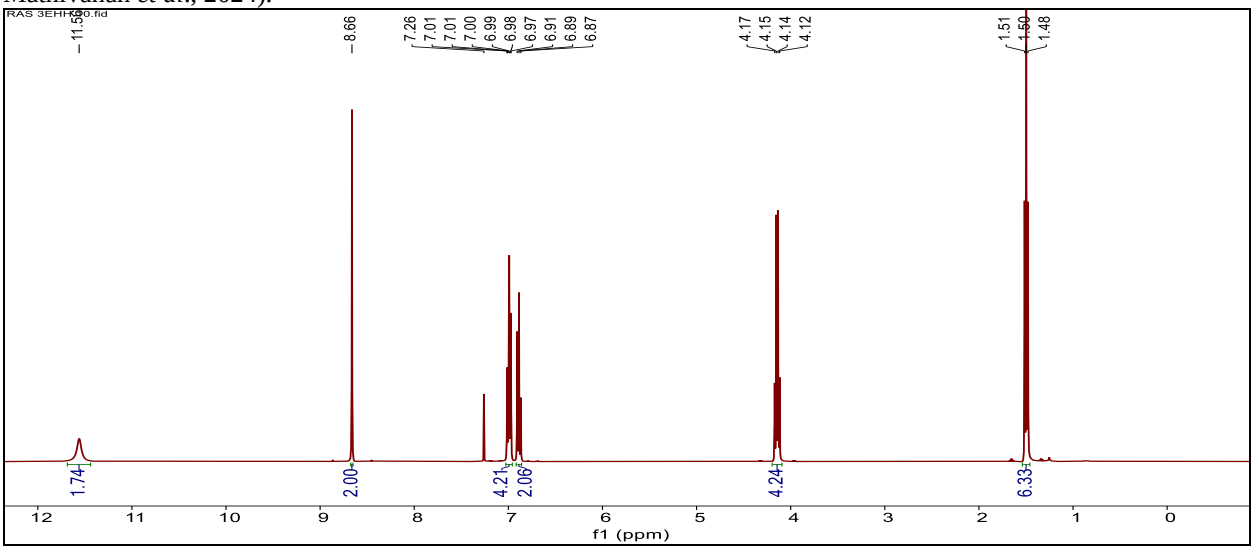

Figure 1: ^{1}H NMR spectrum of 3EHH (400 MHz, $CDCl_3$)

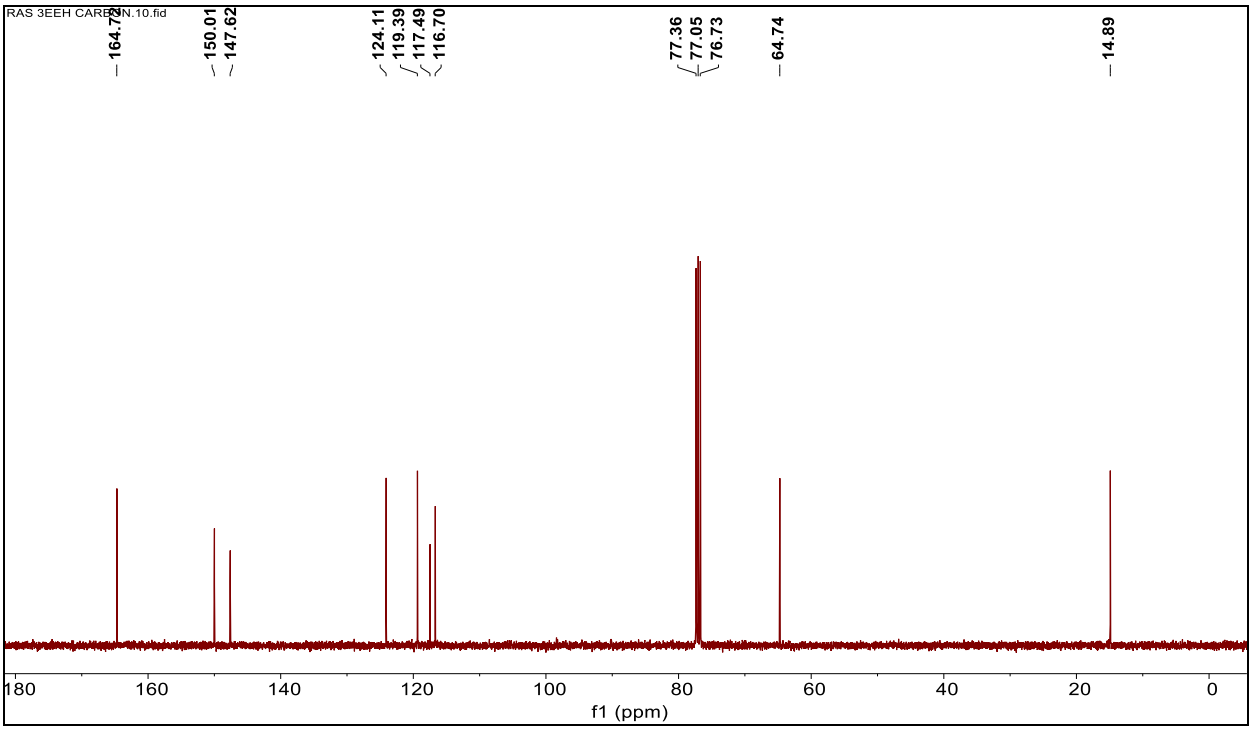

Figure 2: ^{13}C NMR spectrum of 3EHH (400 MHz, $CDCl_3$)

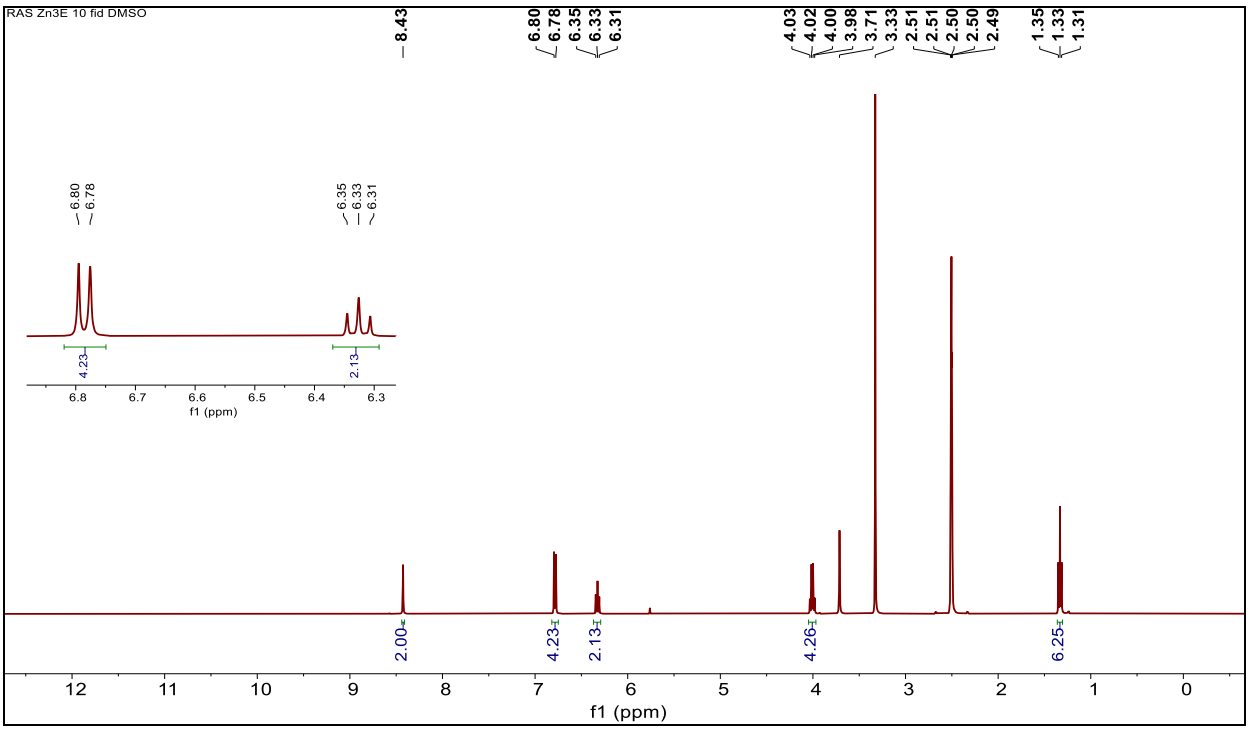

Figure 3: ^{1}H NMR spectrum of Zn3E (400 MHz, DMSO-d_6)

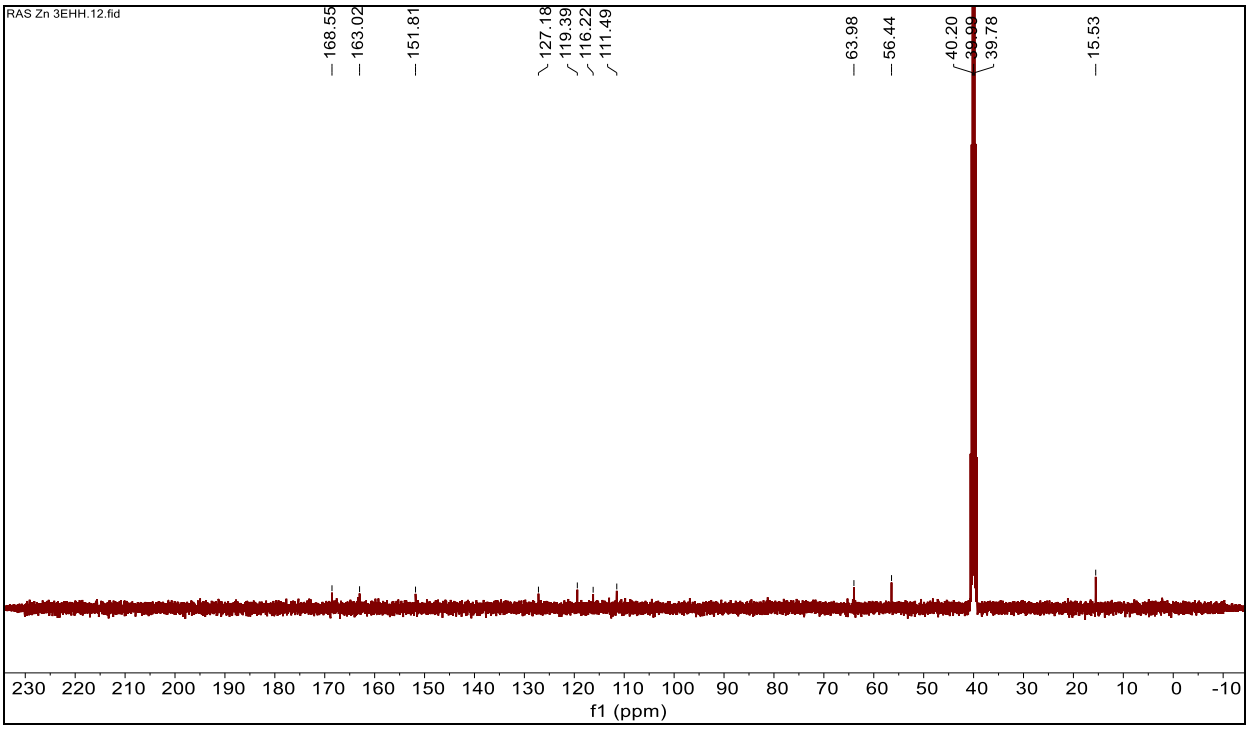

Figure 4: ^{13}C NMR spectrum of Zn3E (400 MHz, DMSO-d_6)

Infrared spectra

The infrared spectral data of the compounds were recorded in **Table 2**. The weak, broad band in **3EHH** due to phenolic υ(O–H) was observed at 3503 cm^{-1}. Similar, but more distinct bands observed in **Cu3E** and **Zn3E** in the range of 3520–3338 cm^{-1}, were assigned to υ(O–H) of lattice water, however, these were absent in **Ag$_2$3E**.

The medium band of C=N frequency in the ligand was found at 1622 cm^{-1}, and was shifted to 1631–1616 cm^{-1} in the complexes, indicating the participation of the azomethine nitrogen in coordination. The benzyl C=C stretch occurred around 1580 cm^{-1}, while the strong band in the 735 cm^{-1} region was assigned to the out-of-plane C–H bending vibration in the *ortho*- and *meta*-substituted aromatic rings. The bands at 1339 and 1214 cm^{-1} were respectively assigned to υ(C–O) of the ethoxy and phenol in **3EHH**. While the former remained relatively unchanged in the complexes, the phenol C–O frequency became lowered to 1205–1193 cm^{-1} after coordination. This confirmed the bond formation to the metal ions through the phenolate oxygen. Liu *et al.* (2015) described a pentanuclear Zn(II) complex containing acetate bridges. In contrast, the absence of acetate bands in **Zn3E**, likely due to the basic reaction conditions, would favour deprotonation of the phenolic oxygen. This was supported by the ^{1}H NMR spectrum and suggests the formation of a simpler mononuclear structure. Metal-to-oxygen and metal-to- nitrogen stretches were allocated to new bands found in the regions 555–506 cm^{-1} and 468–454 cm^{-1}, which were not observed in the free ligand spectrum.

Table 2: Infrared frequencies of the compounds (cm^{-1})

Compounds	***υ*(O–H/H$_2$O)**	***υ*(C=N), *υ*(C=C)**	***υ*(C–O)**	***υ*(M–O/N)**
3EHH	3503	1622, 1577, 735	1339, 1214	----
Cu3E	3490, 3409	1631, 1576, 732	1349, 1205	530, 461
Zn3E	3520, 3338	1616, 1586, 731	1340, 1210	555, 454
Ag$_2$3E	----	1620, 1580, 731	1338, 1193	506, 457

Electronic spectra and magnetic moments

The UV/Visible spectral data and magnetic moments of **3EHH** and the metal complexes are presented in **Table 3**. The yellow ligand exhibited characteristic intraligand absorptions at 272, 287 and 296 nm, assigned to π→π* transitions in the conjugated aromatic system. These bands were slightly shifted in the complexes. The band at 387 nm was assigned to an n → π* transition involving the promotion of the lone pairs of the phenolic oxygen and azine nitrogen atoms to the antibonding π* orbital of

the C=N-N=C chromophore. The presence of the electron-donating ethoxy group and hydrogen bonding contributed to the bathochromic shift of this band to the near-UV region (Kargar *et al.*, 2022).

On coordination, this band was shifted in **Cu3E** and **Zn3E**, while it disappeared in **$Ag_2$3E**, indicative of nitrogen lone-pair donation to the metal centre and in consistence with analogous phenolic Schiff base systems (Loginova *et al.*, 2022). A new band of a higher intensity appeared in the complexes spectra in the range of 405–423 nm, and was assigned to a ligand-to-metal charge transfer (LMCT) transition from the deprotonated phenolate oxygen and azine nitrogen atoms to the empty orbital of the metal ions. **Cu3E** displayed a broad band at 662 nm, assigned to d → d transition of the Cu(II) d^9 centre, which could be assigned to a distorted square planar geometry in which Jahn–Teller distortion lifts the e_g degeneracy and gives rise to a $^2E_g \rightarrow {}^2T_{2g}$ transition. **Zn3E** and **$Ag_2$3E** did not exhibit any band in the visible region, as expected for d^{10} systems, hence, the yellow and pale green colours shown by these complexes, respectively, could be attributed to their LMCT transitions. The room-temperature magnetic moment of 1.50 BM for **Cu3E** confirmed its paramagnetic nature, though lower than the spin-only value for a one-electron system. This could be attributed to spin–orbit coupling contributions inherent in a d^9 configuration and has been reported across structurally related copper(II) complexes (Kargar *et al.*, 2022; Calvo *et al.*, 2023). **Zn3E** and **$Ag_2$3E** complexes were however found to be diamagnetic, as usually observed in d^{10} metal ions.

Table 3: UV/Visible transitions in cm^{-1} (nm) and magnetic moments

Compounds	3EHH	Cu3E	Zn3E	$Ag_2$3E
$\pi \rightarrow \pi^*$	36,760 (272)	37,313 (268)	37,313 (268)	37,453 (267)
$\pi \rightarrow \pi^*$	34,843 (287)	34,965 (286)	34,965 (286)	33,670 (297)
$\pi \rightarrow \pi^*$	33,784 (296)	34,247 (292)	34,130 (293)	33,333 (300)
$n \rightarrow \pi^*$	25,840 (387)	25,707 (389)	26,247 (381)	----
LMCT	----	23,641 (423)	23,697 (422)	24,690 (405)
$d \rightarrow d$	----	15,106 (662)	----	----
μ_{eff} (BM)	----	1.50	D	D

LMCT, ligand-to-metal charge transfer; D, Diamagnetic

IN VITRO ANTIMICROBIAL ACTIVITY

The diameters of inhibition zones from the *in vitro* antimicrobial assays of the compounds at 2 and 4 mg/mL concentrations, were recorded in **Table 4**. The compounds were generally active against the tested bacterial strains (*Staphylococcus aureus*, *Bacillus subtilis*, *Escherichia coli*, *Pseudomonas aeruginosa*, *Klebsiella pneumoniae*, *Salmonella typhi*) and fungal strains (*Candida albicans*, *Trichophyton rubrum*), with inhibitory zones ranging from 8 to 24 mm. While the complexes were more active than **3EHH**, and the activity improved at a higher concentration, however, *Pseudomonas aeruginosa* was resistant to **Zn3E** as shown by a 0 mm inhibition diameter. The **Cu3E** and **$Ag_2$3E** complexes were seen to show broad-spectrum activity against both the bacterial and fungal strains.

The minimum inhibitory and microbiocidal concentrations of the compounds were recorded in **Table 5**. The **$Ag_2$3EH** complex demonstrated highest potency with the lowest MIC of 0.125 mg/mL against both *Bacillus subtilis* and *Salmonella typhi*. Similarly, a [Cu(3EH)] complex showed strong broad-spectrum efficacy with an MIC of 0.25 mg/mL against *Bacillus subtilis*, *Klebsiella pneumoniae*, *Salmonella typhi*, and *Trichophyton rubrum*. While the metal complexes frequently exhibited superior MIC values, the free ligand **3EHH** demonstrated the largest overall individual inhibition zone of 24 mm against *Staphylococcus aureus* at 2 mg/mL. Among the compounds, **Cu3E** and **$Ag_2$3E** complexes demonstrated the largest inhibition zones of 20 mm against multiple strains, including *Staphylococcus aureus*, *Escherichia coli*, *Klebsiella pneumoniae*, and *Salmonella typhi* at 4 mg/mL. The **$Ag_2$3E** the most potent maximum microbiocidal concentration (MMC) of 0.25 mg/mL against *Bacillus subtilis*, representing a significant enhancement over the 4 mg/mL MMC of the ligand. Additionally, **Cu3E** achieving optimal MMC values of 0.25 mg/mL against the fungus *Trichophyton rubrum* and 0.5 mg/mL against both *Klebsiella pneumoniae* and *Candida albicans*.

Table 4: Zones of inhibition of the compounds (mm) against selected bacteria and fungi

Compounds	mg/mL	Bacteria						Fungi	
		S. a	*B. s*	*E. c*	*P. a*	*K. p*	*S. t*	*C. a*	*T. r*
3EHH	4	24	10	15	17	12	20	15	15

	2	16	9	10	13	10	15	10	11
Cu3E	4	20	17	17	17	20	20	20	19
	2	14	15	16	15	15	13	14	16
Zn3E	4	12	19	15	0	14	10	13	12
	2	10	14	14	0	12	0	10	10
$Ag_2$3E	4	12	19	20	12	20	14	10	12
	2	8	16	17	10	17	11	0	10
Control	DMF	R	R	R	R	R	R	R	R
	CIP	19	12	18	14	10	12	NA	NA
	KET	NA	NA	NA	NA	NA	NA	20	22

S.a, Staphylococcus aureus ATCC 6571*; B.s, Bacillus subtilis* ATCC 3366*; E.c, Escherichia coli* ATCC 25922*; P.a, Pseudomonas aeruginosa* ATCC 27853*; K.p, Klebsiella pneumoniae* ATCC 700303*; S.t, Salmonella typhi* ATCC 14028*; C.a, Candida albicans; T.r, Trichophyton rubrumi;* CIP, Ciprofloxacin; KET, Ketoconazole; NA = Not applicable

Table 5: Minimum Inhibitory Concentration and Minimum Microbiocidal Concentration in mg/mL

Compounds		Bacteria						Fungi	
		S. a	*B. s*	*E. c*	*P. a*	*K. p*	*S. t*	*C. a*	*T. r*
3EHH	MIC	2.5	4	2	0.5	1	0.5	0.5	1
	MMC	2.5	4	4	2	4	0.5	1	2
Cu3E	MIC	0.5	0.25	0.5	1	0.25	0.25	1	0.25
	MMC	1	2	2	1	0.5	1	0.5	0.25
Zn3E	MIC	1	0.5	0.5	>4	1	>4	4	2
	MMC	2	1	2	>4	1	>4	2	4
$Ag_2$3E	MIC	1	0.125	0.25	2	0.25	0.125	4	4
	MMC	2	0.25	1	4	0.5	1	>4	4
CIP	MIC	5	5	10	>10	10	10	NA	NA
	MMC	5	10	10	>10	10	>10	NA	NA
KET 1%	MIC	NA	NA	NA	NA	NA	NA	0.25	1
	MMC	NA	NA	NA	NA	NA	NA	5	1

DPPH radical scavenging activity

The results of the DPPH radical scavenging assay were recorded in **Table 6**. The ligand **3EHH** achieved a maximum inhibition of 56.77 ± 0.10% at 1000 µg/mL, corresponding to an IC_{50} of 486.82 µg/mL. This moderate activity reflected the contribution of the phenolic –OH group of the 3-ethoxy-2-hydroxybenzaldehyde moiety, which serves as the primary hydrogen-atom donor, supplemented by the electron-rich *bis*-azomethine bridge. The electron-donating ethoxy substituent at the 3-position augments the electron density at the reactive hydroxyl oxygen, yet the absence of multiple hydroxyl groups limits the overall radical quenching capacity of the free ligand, compared to ascorbic acid.

Upon coordination to metal centres, the scavenging activity improved remarkedly for the complexes, following the order: **Cu3E** (IC_{50} 138.62 µg/mL) ≈ **Zn3E** (IC_{50} 139.45 µg/mL) > **$Ag_2$3E** (IC_{50} 353.34 µg/mL) > **3EHH** (IC_{50} = 486.82 µg/mL), as summarised in **Table 6**.

The copper(II) complexes exhibited the most pronounced enhancement, reflecting the redox versatility of Cu^{2+}/Cu^{+} that enables direct electron transfer to DPPH radicals (Cai *et al.*, 2006). Coordination also deprotonates the phenolic oxygen to generate a phenolate, intrinsically a stronger reductant than the parent phenol, and enforces planarity across the chelate ring, maximising π-conjugation and stabilising the radical intermediate formed after hydrogen donation (Tezcan *et al.*, 2021).

The **Zn3E** complex performed comparably to **Cu3E** despite Zn^{2+} being redox-inactive, confirming that the scavenging enhancement in this case is ligand-mediated,

driven by metal-induced electron delocalisation across the chelated π-framework rather than metal-centred electron transfer (Subramanian *et al.*, 2019). The **$Ag_2$3E** though improved over the free ligand, showed the smallest gain among the complexes, likely because the preference of Ag(I) for linear coordination limits the degree of chelate planarity and conjugation achievable in the complex.

Table 6: *IC_{50} values from the DPPH radical scavenging assay*

Compound	IC_{50} (µg/mL)	Relative Potency vs. 3EHH
Ascorbic acid	9.62	50.6×
3EHH	486.82	1.00 (reference)
Cu3E	138.62	3.51×
Zn3E	139.45	3.49×
$Ag_2$3E	353.34	1.38×

Ferric Reducing Antioxidant Power (FRAP)

The FRAP values of the compounds were recorded in **Table 7**. At 1000 µg/mL, the ranking of ferric reducing power was: **Zn3E** (22.89 ± 0.11) > **Cu3E** (18.59 ± 0.51) > **$Ag_2$3E** (13.92 ± 0.09) > **3EHH** (9.24 ± 0.03) AAE mg/g, as presented in Table 4.2.

The free ligand showed the lowest activity, while all complexes were significantly more potent. Strikingly, **Zn3E** showed the highest FRAP. This divergence is mechanistically coherent: FRAP operates under mildly acidic conditions where ligand-mediated electron donation into the Fe^{3+} pool dominates, and here the total electron density of the coordinated ligand framework is the decisive factor. Without competing metal-radical side reactions, the Zn(II)–3EHH system channels the full polarising effect of metal coordination into enhancing ligand electron availability, producing the highest reducing capacity in the series. This interpretation aligns with the work of Subramanian *et al* (2019), who reported analogous DPPH/FRAP rank reversals in zinc and copper hydrazone complexes and attributed them to the same mechanistic distinction.

Table 7: Ferric Reducing Antioxidant Power (FRAP) values of the compounds at 1000 µg/mL, expressed as Ascorbic Acid Equivalent (AAE mg/g)

Compound	FRAP (AAE mg/g) at 1000 µg/mL	Enhancement Factor vs. 3EHH
3EHH	9.240 ± 0.032	1.00 (reference)
Cu3E	18.587 ± 0.512	2.01×
Zn3E	22.890 ± 0.113	2.48×
$Ag_2$3E	13.920 ± 0.091	1.51×

CONCLUSION

The aldazine ligand, **3EHH**, and its Cu(II), Zn(II), and Ag(I) complexes were synthesised under refluxing conditions and characterised. Spectroscopic data supported tetradentate N_2O_2 coordination of the ligand to Cu(II) and Zn(II) through the azine nitrogen and phenolic oxygen, in distorted square planar geometries, and NO coordination for dinuclear Ag(I) with linear geometry.

The metal complexes exhibited broad-spectrum antimicrobial activity, with Cu(II) and Ag(I) complexes showing the highest inhibition zones up to 20 mm. Antioxidant activity, measured through the DPPH radical scavenging and FRAP assays, was also enhanced upon complexation, with Cu(II) and Zn(II) complexes being the most active. These results indicated that metal chelation improved the biological potential of 3EHH, and both Cu(II) and Zn(II) complexes could be further explored as antimicrobial and antioxidant agents.

CONFLICT OF INTEREST

The authors declare there are no conflicts of interest.

REFERENCE

Aazam, E. S., Majrashi, M., and Hussien, M. A. (2024). Exploring novel NH-form resorcinol-based Schiff base and its metal complexes: Synthesis, characterization, cytotoxic activity, molecular docking and ADME studies. *Heliyon*, 10 (18), e37385. https://doi.org/10.1016/j.heliyon.2024.e37385

Blois, M. S. (1958). Antioxidant determinations by the use of a stable free radical. *Nature*, 181, (4617), 1199–1200. https://doi.org/10.1038/1811199a0

Brand-Williams, W., Cuvelier, M. E., and Berset, C. (1995). Use of a free radical method to evaluate

antioxidant activity. *LWT - Food Science and Technology*, 28(1), 25–30. https://doi.org/10.1016/S0023-6438(95)80008-5

Cai, Y., Luo, Q., Sun, M., and Corke, H. (2006). Antioxidant activity and phenolic compounds of 112 traditional Chinese medicinal plants associated with anticancer. *Life Sciences*, 74(17), 2157–2184.

Calvo, R., Sartoris, R. P., Nascimento, O. R., Šedivý, M., Sojka, A., Neugebauer, P., & Santana, V. T. (2023). Quantum phase transitions probed by EPR spectra in dimeric spin arrays with supramolecular couplings. Coordination Chemistry Reviews, 480, 215007. https://doi.org/10.1016/j.ccr.2022.215007

Chosenyah, M., Swaraj, R., Novikov, V., Maydykovskiy, A., Khapre, A., Murzina, T., and Chandrasekar, R. (2026). Dynamic Crystal Photonics: Mechanically Mobile Organic Nonlinear Optical Microring Resonators. *Journal of the American Chemical Society*, 148 (5): 5252 – 5243. https://doi.org/10.1021/jacs.5c17711

Chouiter, A. D., Mousser, M. O., Mousser, H. B., Krid, A., Belkhiri, L., Fleutot, S., and Francois, M. (2023). Synthesis, spectra, crystal, DFT, molecular docking and *in vitro* cholinesterase inhibition evaluation on two novel symmetrical azine Schiff bases. *Journal of Molecular Structure*, 1281, 135171. https://doi.org/10.1016/j.molstruc.2023.135171

Dhanya, T.M., Prathapachandra K. M., Rajimon, K.J., Anjali K. G., Varughese, J.K., Raghu, K.G., Philip, S., Divya, K.M., Augustine, M., and Mohanan, P.V. (2025). Unveiling the multifaceted bioactivity of copper(II)-Schiff base complexes: a comprehensive study of antioxidant, anti-bacterial, anti-inflammatory, enzyme inhibition and cytotoxic potentials with DFT insights. *Dalton transactions* 54 (8): 3216–3234. https://doi.org/10.1039/d4dt02486a

Ganesan, V., Govindasamy, C., Shanmugasundaram, E., Vellaisamy, K., Krishnan, N. K., Mani, M. K., Kaliyamoorthy, S., Liu, B.-T., and Thambusamy, S. (2024). 2-Hydroxybenzaldehyde Azine and γ-Cyclodextrin Based Colorimetric/Fluorescent Probe for Highly Sensitive and Selective Detection of Cu^{2+}. *ChemPhotoChem*, 8(12), e202400170. https://doi.org/10.1002/cptc.202400170

Gorokhov, V.Y., Zabolotnykh, S.A., Chekanova, L.G., and Vaulina, V. N. (2024). New Method for the Synthesis of Ald(ket)azines and their Antioxidant Activity. *Eurasian Journal of Chemistry* volume 29 (4 (116)), 4–12. https://doi.org/10.31489/2959-0663/4-24-7

Hadigheh Rezvan, V., Aminivand, Y. DFT computational study of optical properties for *bis*-Schiff bases of 8-aminoquinoline derivatives and furan-2, 3-di-carbaldehyde. *Structural Chemistry* **35**, 1577–1587 (2024). https://doi.org/10.1007/s11224-024-02296-3

Hasan, A.W., Zubaidi, Z.N., Mustafa, M.Y. Synthesis, characterization, DFT calculation, and biological activity of a new Schiff base ligand and its ZnO and Co_3O_4 nano-metal oxide complexes. *BMC Chemistry* **20**, 10 (2026). https://doi.org/10.1186/s13065-025-01673-1

Kargar, H., Ashfaq, M., Fallah-Mehrjardi, M., Behjatmanesh-Ardakani, R., Munawar, K. S., & Tahir, M. N. (2022). Synthesis, crystal structure, spectral characterization, theoretical and computational studies of Ni(II), Cu(II) and Zn(II) complexes incorporating Schiff base ligand derived from 4-(diethylamino)salicylaldehyde. Inorganica Chimica Acta, 536, 120878. https://doi.org/10.1016/j.ica.2022.120878

Karimian, S., Kazemi, F., Attarroshan, M., Gholampour, M., Hemmati, S., Sakhteman, A., Behzadipour, Y., Kabiri, M., Iraji, A., and Khoshneviszadeh, M. (2021). Design, synthesis, and biological evaluation of symmetrical azine derivatives as novel tyrosinase inhibitors. *BMC Chemistry*, *15*, 54 (2021). https://doi.org/10.1186/s13065-021-00780-z

Liu, E., Zhang, Y. Z., Tan, J., Yang, C., Li, L., Golen, J. A., Rheingold, A. L., and Zhang, G. (2015). Zn(II) and Co(III) metallosupramolecular assemblies derived from a rigid bis-Schiff base ligand. *Polyhedron*, 102, 41-47. https://doi.org/10.1016/j.poly.2015.07.074

Liu, J., Leng, C.C., Chen, Q., Liang, Q., Li, C., Li, S., Zhang, Z., and Xiao, L. (2022). A Novel AIE Fluorescent Probe for Cu2+ Recognition Based on Salicylaldehyde-azine System. *ChemistrySelect*, 7, e202203313. https://doi.org/10.1002/slct.202203313

Loginova, N., Gvozdev, M., Osipovich, N., Khodosovskaya, A., Koval'chuk-Rabchinskaya, T., Ksendzova, G., Kotsikau, D., & Evtushenkov, A. (2022). Silver(I) complexes with phenolic Schiff bases: synthesis, antibacterial evaluation and interaction with biomolecules. *ADMET and DMPK*, 10(3), 209–227. https://doi.org/10.5599/admet.1167

Mathivanan, M., Shanmugaraj, K., Ilanchelian, M., Haribabu, J., Hidalgo, P. I., and Novoa, N. (2024). 3-Ethoxysalicylaldimine-based symmetrical azine-linked luminogen exhibiting ESIPT and bright orange colour AIE behaviour with live cell bioimaging application. *Luminescence*, 39(9), e4892. https://doi.org/10.1002/bio.4892

Manzocco, L., Anese, M., and Nicoli, M. C. (1998). Antioxidant properties of tea extracts as affected by processing. *LWT - Food Science and Technology*, 31(7-8), 694–698. https://doi.org/10.1006/fstl.1998.0491

Naito, M., Tsukamoto, M., Gonnai, K., Takaya, H., Miyagawa, S., Sakaguchi, T., and Hashimoto, T. (2025). Synthesis, structure and solid state emission properties of 6-alkoxysalicylaldehyde azines. *Journal of Molecular Structure*, 1329, 141322. https://doi.org/10.1016/j.molstruc.2025.141322

National Committee for Clinical Laboratory Standards (NCCLS). (1999). *Methods for determining bactericidal activity of antimicrobial agents; approved guideline* (NCCLS document M26-A).

National Committee for Clinical Laboratory Standards (NCCLS). (2002). *Reference method for broth dilution antifungal susceptibility testing of yeasts; approved standard—second edition* (NCCLS document M27-A2).
Oyaizu, M. (1986). Studies on products of browning reaction: Antioxidative activities of products of browning reaction prepared from glucosamine. *Japanese Journal of Nutrition*, 44(6), 307–315. https://doi.org/10.5264/eiyogakuzashi.44.307

Rabiei, K., Mohammadkhani, Z., Keypour, H., and Kouhdareh, J. (2023). Palladium Schiff base complex-modified Cu(BDC-NH_2) metal-organic frameworks for C-N coupling. *RSC Advances*, *13*(12), 8114–8129. https://doi.org/10.1039/d3ra01020a

Rajadurai, D., Al-Hussain, S.A., Elangovan, N. *et al.* Design, Synthesis, and Fluorescence Properties of *Bis*-Schiff Base Derivatives Via Spectroscopic, Computational, and Docking Approaches. *Journal of Fluorescence* **36**, 1879–1911 (2026). https://doi.org/10.1007/s10895-025-04693-1

Rani, A., Sharma, J., Ramasamy, S.K., and Aman, S. (2026). Schiff Base Metal Complexes as Dual Antimicrobial and Anticancer Agents: Synthesis, Characterization, DFT, and Molecular Docking Investigations. *ChemistrySelect* 11, no. 2: e05632. https://doi.org/10.1002/slct.202505632

Sahu, M., Manna, A. K., and Patra, G. K. (2022). A fluorescent colorimetric vanillin di-Schiff base chemosensor for detection of Cu(II) and isolation of trinuclear Cu(II)–dihydrazide. *Materials Advances*, 3(5), 2495–2504. https://doi.org/10.1039/d1ma01227d

Saulawa, A. I., Dangani, A. H., & Muhammad, S. (2024). Synthesis, Characterization, and Antibacterial Evaluation of Divalent Metal Complexes of Schiff Base [(4-Methoxy- Benzylidene)- Amino]-Acetic Acid. *Journal of Basics and Applied Sciences Research*, *2*(1), 195–199. https://doi.org/10.33003/jobasr-2024-v2i1-45

Shaaban, S., Abu-Dief, A. M., Alaasar, M., Al-Janabi, A. S. M., Alsadun, N. S., Al Duaij, O. K., and Yousef, T. A. (2025). Novel Fe(III), Cu(II), and Zn(II) chelates of organoselenium-based Schiff base: Design, synthesis, characterization, DFT, anticancer, antimicrobial, and antioxidant investigations. *Applied Organometallic Chemistry*, 39(1), e7776. https://doi.org/10.1002/aoc.7776

Taha, M., Rahim, F., Zaman, K., Anouar, E. H., Uddin, N., Nawaz, F., Sajid, M., Khan, K. M., Shah, A. A., Wadood, A., Rehman, A. U., and Alhibshi, A. H. (2023). Synthesis, in vitro biological screening and docking study of benzooxazole bis Schiff base derivatives as a potent anti-Alzheimer agent. *Journal of Biomolecular Structure and Dynamics*, 41(5), 1649–1664. http://dx.doi.org/10.1080/07391102.2021.2023640

Thakor, P.M., Patel, J.D., Patel, R.J., Chaki, S.H., Khimani, A.J., Vaidya, Y.H., Chauhan, A.P., Dholakia, A.B., Patel, V.C., Patel, A.J., Bhavsar, N., and Patel, H.V. (2024). Exploring New Schiff Bases: Synthesis, Characterization, and Multifaceted Analysis for Biomedical Applications. *ACS Omega*, *9*, 35431 - 35448. https://doi.org/10.1021/acsomega.4c02007